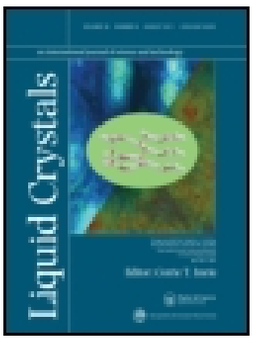

Liquid Crystals

ISSN: 0267-8292 (Print) 1366-5855 (Online) Journal homepage: https://www.tandfonline.com/loi/tlct20

A three-layer egg-configurated Bragg microcavity of polyglycerol coated cholesteric-liquid-crystal encapsulated by hollow-glass-microsphere

Jianyang Hu, Dongying Fu, Chunli Xia, Chi Zhang, Lishuang Yao, Chunlian Lu, Weimin Sun & Yongjun Liu

To cite this article: Jianyang Hu, Dongying Fu, Chunli Xia, Chi Zhang, Lishuang Yao, Chunlian Lu, Weimin Sun & Yongjun Liu (2019): A three-layer egg-configurated Bragg microcavity of polyglycerol coated cholesteric-liquid-crystal encapsulated by hollow-glass-microsphere, Liquid Crystals, DOI: 10.1080/02678292.2019.1660426

To link to this article: https://doi.org/10.1080/02678292.2019.1660426

LIQUID CRYSTALS
https://doi.org/10.1080/02678292.2019.1660426

Taylor & Francis
Taylor & Francis Group

A three-layer egg-configurated Bragg microcavity of polyglycerol coated cholesteric-liquid-crystal encapsulated by hollow-glass-microsphere

Jianyang Hu[a], Dongying Fu[a], Chunli Xia[a], Chi Zhang[a], Lishuang Yao[b,c], Chunlian Lu[a], Weimin Sun[a] and Yongjun Liu[a,b]

[a]Key Lab of In-fiber Integrated Optics, Ministry Education of China, Harbin Engineering University, Harbin, China; [b]State Key Laboratory of Applied Optics, Changchun Institute of Optics, Fine Mechanics and Physics, Chinese Academy of Sciences, Changchun, China; [c]Department of Physics, College of Science, Shantou University, Shantou, China

ABSTRACT

This letter reports the optical pumped lasing behaviours of a three-layer Bragg resonance cavity consisting of dye-doped cholesteric liquid crystal (DDCLC) microdroplet, polyglycerol-2 and hollow glass microsphere. The function of PG2 is to control the parallel anchoring of the liquid crystal (LC) molecules on the surface of the LC microdroplet. The whispering-gallery mode (WGM), radial Bragg (photonic bandgap, PBG) mode and Bragg WGM (BWGM) are observed in DDCLC microspheres with different helical pitches and LC refractive indices. The formation mechanisms of six types of lasing emission conditions are analysed in detail. The study results present the prospect of controlling the output mode of the laser. Furthermore, such solid shell-based DDCLC microspheres have outstanding potential applications in miniaturised 3D Bragg lasers, sensors, and integrated and tunable optical devices.

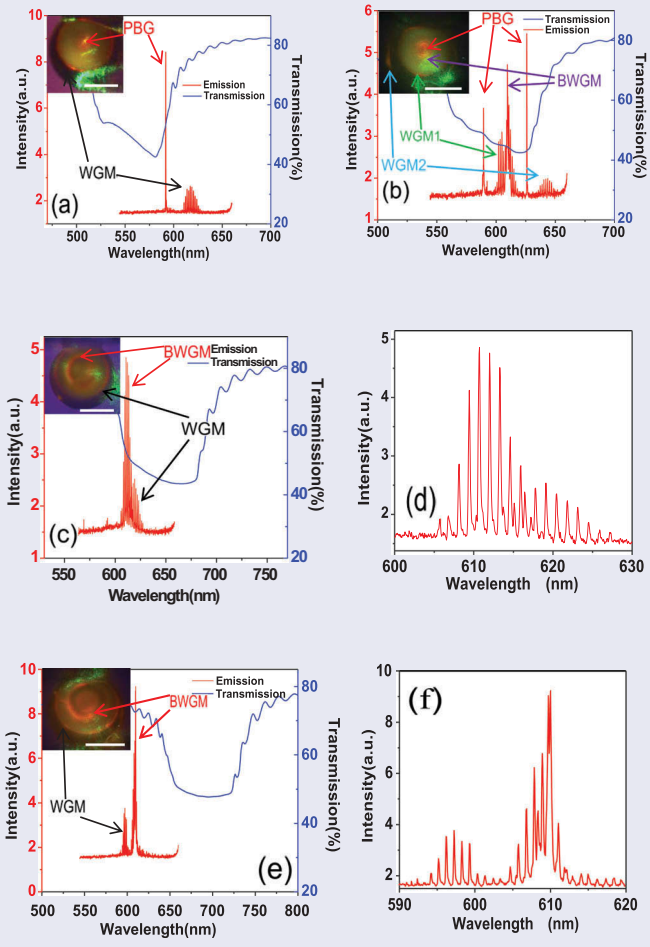

ARTICLE HISTORY
Received 9 July 2019
Accepted 22 August 2019

KEYWORDS
Cholesteric liquid crystal; whispering-gallery mode; Bragg lasing mode; microlaser

CONTACT Yongjun Liu liuyj@hrbeu.edu.cn

1. Introduction

Liquid crystals (LCs) have received great attention in various liquid crystal displays and photonic applications due to their remarkable molecular reconfiguration ability and excellent responsiveness to external fields [1–3]. The cholesteric liquid crystals (CLC) own many unique and interesting properties due to their typical self-organised photonic superstructure. Therefore, CLC has great application potential in LC lasers and have attracted a lot of attention [4,5]. The CLC is formed by self-organisation of rod-like liquid crystal molecules. The chiral dopants provide self-assembly abilities to continuously rotate liquid crystal molecules to an angle of 2π along the helical axis [6]. The CLC can be considered as a mirrorless one-dimensional photonic bandgap (PBG) microcavity due to its periodic dielectric helical structure [5]. The fluorescent dye-doped cholesteric liquid crystal (DDCLC) produce the low-threshold lasing emission along the helical axis by appropriate optical pumping, because the spontaneously emitted fluorescence from the dye is suppressed within the stop band and enhanced at the band edges [7]. DDCLC lasers have been extensively studied for their simply fabrication process and superior tunabilities. Pitch tunable DDCLC lasers based on element [8], temperature [9], voltage [10,11], shape-reconfiguration [12] and light [13,14] have been reported.

Since LC material is a soft matter, a perfect spherical LC microdroplet with the outstandingly smooth surface can be naturally formed by surface tension. At present, the LC microdroplets have been successfully applied to temperature detection [15], electrical measurement [16] and biosensor [17]. In addition, a CLC microdroplet can confine light within its tiny microsphere volume to produce CLC microdroplet laser by total internal reflection at the interface between CLC and the environment or by Bragg reflection from the periodic dielectric helical structure of CLC. Therefore, a considerable research effort has been conducted on CLC microdroplet lasers. The lasing caused by the mechanism of total internal reflection at the interface is called the whispering-gallery mode (WGM) lasing. A DDCLC microdroplet with alternating high and low refractive index layers can be treated as a three-dimensional (3D) Bragg cavity. This mirrorless 3D Bragg cavity is capable of trapping light in all directions without considering the direction of light propagation [18]. Therefore, many researchers have focused their attention on the Bragg cavity-based DDCLC microdroplet. The WGM and PBG mode lasers have been reported, in which the DDCLC microspheres are prepared by mechanically mixing DDCLC with an immiscible fluid [16,19,20], pumping DDCLC through a tapered microtube [21] or coating the silica-glass-microspheres with DDCLC [4]. However, there are several issues that limit the practical applications of these CLC microdroplet lasers. The most prominent issue is the instability and contamination of the liquid surface. Second, numerous CLC microdroplets would cause spectral overlap. Finally, it is difficult to achieve miniaturisation.

In this letter, we design and fabricate a three-layer resonance microcavity consisting of DDCLC microdroplet, polyglycerol-2 (PG2) and hollow glass microsphere (HGM). We control the parallel anchoring of the LC molecules on the droplet surface by using PG2, and PG2 has extremely high viscous force to hold CLC microdroplets in HGM. The DDCLC microsphere resonance cavity can be considered as a 3D Bragg cavity. This low cost and easy-produced three-layer resonator shows excellent stability and achieves miniaturisation. When pumped by a pulsed laser, DDCLC microspheres with different refractive indices of LCs and chiral dopant concentrations exhibit the lasing behaviours of WGM, PBG mode and Bragg WGM (BWGM). The formation mechanisms and control methods of WGM, PBG mode and the Bragg WGM in a solid shell-based liquid crystal microsphere are analysed in detail for the first time to our best knowledge.

2. Experiment

Various CLC materials are prepared by doping chiral dopants with different concentrations into two nematic liquid crystals (NLC). NLC BHR32400-200 which has a higher refractive index (n_e = 1.765, n_o = 1.514) shows a phase transition from an anisotropy phase to an isotropic phase at 104°C. Chiral dopants R811 with concentrations of 28wt%, 26wt%, 23wt% and 20wt% are mixed with BHR32400-200 to produce four groups of high refractive index CLCs (HCLC). The other NLC BYLC5214-000 which has a lower refractive index (n_e = 1.566, n_o = 1.418) shows a phase transition from an anisotropy phase to an isotropic phase at 92°C. Three groups of low refractive index CLC (LCLC) mixtures are made by doping chiral dopants R811 with concentrations of 24wt%, 22wt% and 20wt% into BYLC5214-000 (all materials are from BayiSpace, China). Laser dye 4-dicyano-methylene-2-methyl- (6–4-dimethylaminostryl)-4H-pyan (DCM, from Exciton) with a concentration of 1wt% is added into CLCs as a gain

medium. The process for production of the three-layer DDCLC resonance cavity is as follows: First, we use a small piece of single mode fibre as a microsphere holder, and an HGM (n = 1.45, d = 20 to 120 μm, the glass thickness is 900nm, K25, Minnesota Mining and Manufacturing Company) is fixed on the fibre by an ultraviolet curing adhesive (Figure 1(a)). Next, a microhole ($d \approx 10$ μm) is drilled on the surface of the HGM with a sharply tapered fibre. The position was adjusted manually through using a fusion aplicer. Then, PG2 (n = 1.49) is filled into the HGM through a tapered microtube (Figure 1(b)). Finally, DDCLC is injected into the PG2 after a hole is pierced in the centre of PG2 in the same way. The microscopy image of a DDCLC microsphere is shown in Figure 1(c). Figure 1(d) presents a polarised optical microscopy image of a DDCLC microsphere with a Bragg structure. The schematic of the experimental setup is shown in Figure 1. A frequency-doubled Nd:YAG pulsed laser (532 nm, 8 ns pulse duration and 5 Hz repetition rate) is employed as the pumping laser. The pumping laser first passes through a beam splitter and an objective lens (40×), then is coupled into the fibre, and finally illuminates on the microsphere sample to excite the DDCLC material. The spectrum of the excited lasing is detected by spectrometer, and the morphology of the microsphere is observed by an optical microscope. A power metre is used to monitor the pumping laser power.

3. Results and discussion

The lasing spectrum of an HDDCLC (26wt% R811) filled HGM is shown in Figure 2. A typical WGM is formed because the refractive index of CLC is larger than the air and glass [22,23]. The Q factor is 2.6×10^3, and the free spectral range (FSR) is 0.89 nm. Figure 2 (b) presents the expanded spectrum in the range of 613–617 nm. The WGM also can be clearly observed at the interface between the microsphere and the air as shown in the left insets of Figure 2(a). In this case, because the HGM has no surface anchoring ability, the CLC molecules exhibit a chaotic arrangement, this

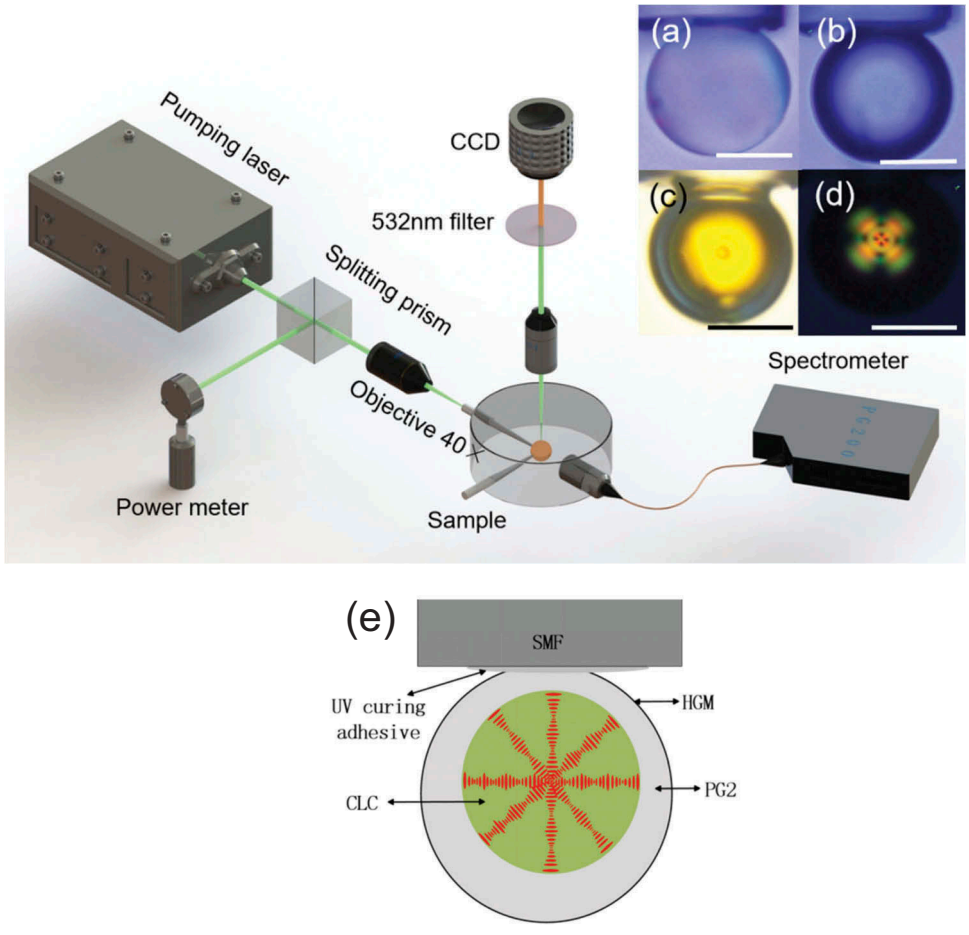

Figure 1. (Colour online) Schematic diagram of the experimental setup. (a) Microscopy image of an HGM, (b) PG2 filled HGM, (c) Microscopy image of a DDCLC microsphere, (d) Polarised optical microscopy image of a DDCLC microsphere, (e) The schematic of the DDCLC microsphere. The scale bar is 50 μm.

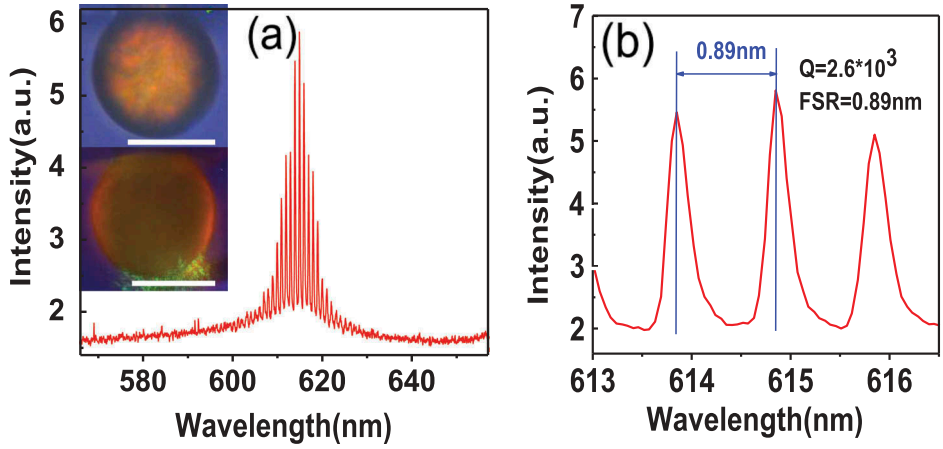

Figure 2. (Colour online) (a) Lasing spectrum of an HGM filled with HDDCLC (26wt%). The top left insets are polarised optical microscopy images of the HGM, the bottom left insets show microscopy images of the pumped HGM. (b) The expanded spectrum in the range of 613–617 nm. The scale bar is 50 μm.

cavity cannot be treated as a Bragg cavity, and the Bragg laser is not excited.

Since PG2 has the ability to control the uniform orientation of LC molecules, when DDCLC is injected into the PG2 filled HGM, it can self-assemble into a radial internal structure in a short time [24,25]. As a result, a DDCLC microsphere Bragg cavity with a radial periodic structure is created, as shown in Figure 1(c,d). According to the principle of Bragg reflection, the reflection band is centred at $\lambda = np$ [26]. The positions of the wavelength edges of the reflection band are $\lambda_1 = n_e p$ and $\lambda_2 = n_o p$, respectively, and the width of the reflection band is $\Delta\lambda = \Delta np$, where birefringence Δn is n_e-n_o, $p = 1/(\beta c)$ is the helical pitch, c is the concentration of the chiral dopant, and β is the helical twisting power (HTP). As shown in Figures 3 and 4 (blue lines), the transmission spectra of CLCs present a significant depression at the position of PBG, and the width of the reflection band expands as the decrease of the concentration of the chiral dopant.

Figure 3 exhibits typical lasing emission spectra (red lines) of HDDCLC microspheres doping with different concentrations of chiral dopants. For the HDDCLC microsphere doped with 28wt% R811(Figure 3(a)), a PBG with a wavelength of 590 nm, which is derived from the 3D Bragg lasing at the centre of the CLC microdroplet, is observed in the lasing spectrum. It presents a bright spot in the inset. In addition, WGMs also appear in the spectrum, which shows a red bright ring on the interface between CLC and PG2 in the inset. We notice that PBG only appears at the long-wavelength edge of the reflection band rather than at both edges. Theoretically, PBGs could occur in both edges of the reflection band. However, the optical gain material used in our experiments is DCM which has a fluorescence emission wavelength of about 600 nm. Only when the wavelength edge of the reflection band is close to the emission wavelength, the edge of the reflection band is amplified, and PBG is generated. The equations in the previous paragraph show that when the concentration of the chiral dopant drops, the helical pitch increases and the wavelength edges of the reflection band are red shifted. Therefore, if both wavelength edges of the reflection band move into the emission wavelength range, two PBGs will be excited. As shown in Figure 3(b), two PBGs with wavelengths of 589 and 625 nm are found in HDDCLC microsphere with 26wt% R811. However, the gain of DCM is asymmetry to PBG wavelength. In our experiments, we find that PBG lasing emission is more powerful in the long-wavelength edge of the reflection band than the short-wavelength edge under the same excitation conditions. Therefore, the PBG intensity at 625 nm is higher than that at 589 nm. Two WGMs are also observed. WGM1 occurs on the interface between CLC and PG2, and WGM2 appears on the interface between PG2 and air. Because most of the fluorescence is confined within the CLC microdroplet, and only a very small amount of light escapes to the outside to generate the second WGM at the air and PG2 interface, this weak WGM2 occasionally appears. In addition to the common WGMs and PBGs, BWGM with a smaller bright ring is noticed in the CLC microdoplert. It is not yet clear what mechanism leads to BWGM. However, the most reasonable explanation is that light is trapped by multiple Bragg reflections in a periodic repeating structure [27]. Similar to WGM, which is induced by total internal reflection at the interface, BWGM is caused by internal Bragg reflection.

In order to better study BWGM, we further reduce the concentration of the chiral dopant to increase the helical pitch. As shown in Figure 3(c, e), PBG is no longer excited, whereas a larger ring is observed in the CLC microdoplert, and a group of spectrum similar to

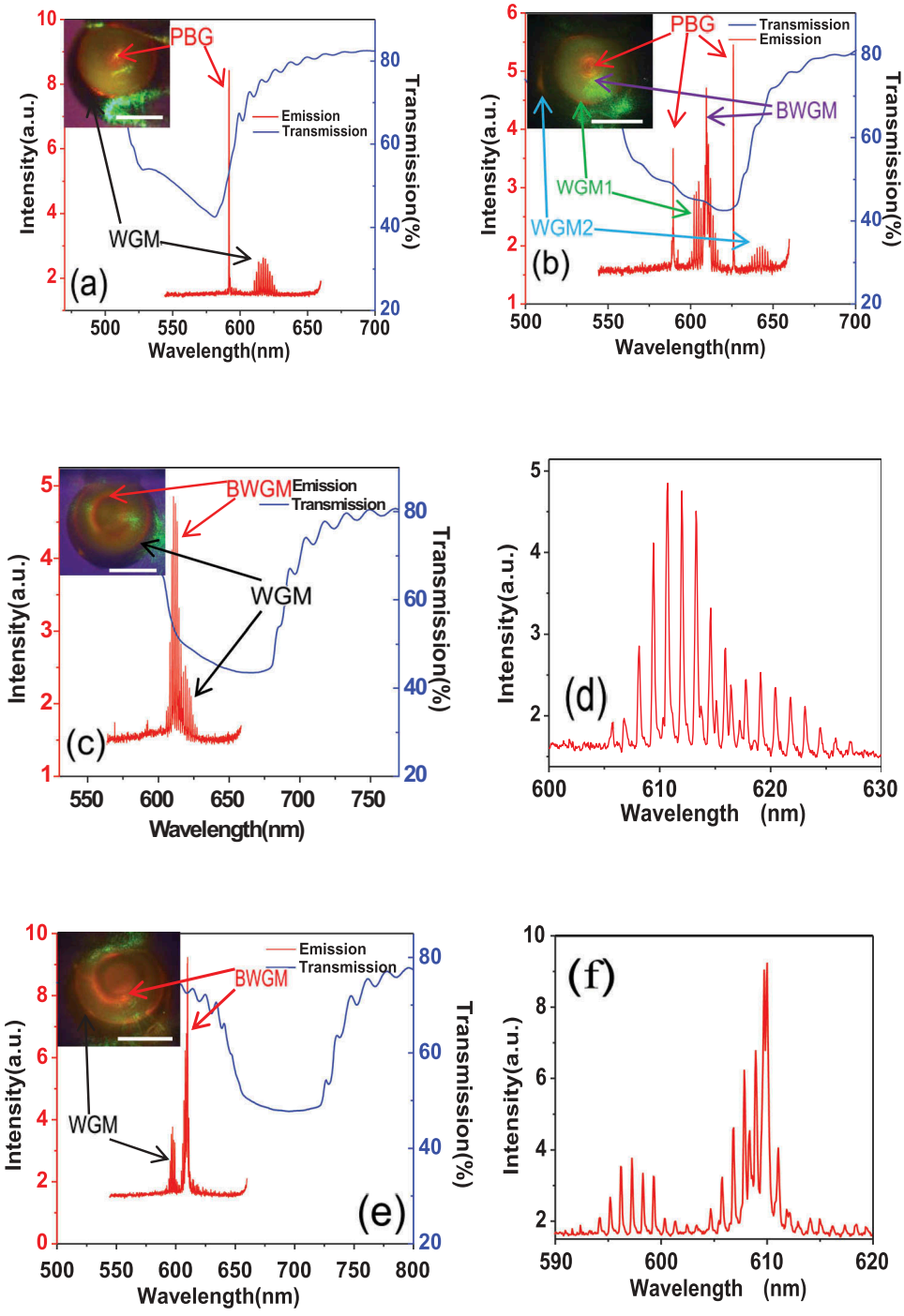

Figure 3. (Colour online) Lasing (red lines) and transmission (blue line) spectra of the pumped HDDCLC microspheres with different chiral dopant concentrations. (a) 28wt%, (b) 26wt%, (c) 23wt% and (e) 20wt%. The top left insets are microscopy images of microspheres. (d), (f) The expanded spectra for identifying two different modes. The scale bar is 50 μm.

WGM is detected, which means that a higher order of BWGM is produced.

To suppress WGMs on the surface of the CLC microdroplet, the refractive index difference between CLC and PG2 should be as small as possible. Therefore, LDDCLC microspheres are applied to the following experiments. As shown in Figure 4, when the LDDCLC microsphere is pumped by a pulsed laser, the bright rings no longer appears on the surface of the CLC microdroplet, and WGMs are invisible in the lasing spectrum, which means WGMs are effectively suppressed. When the LDDLC with a short helical pitch (24wt% R811) is employed, the fluorescence is strongly limited to the centre of the CLC microdroplet and a single PBG at the long-wavelength edge of

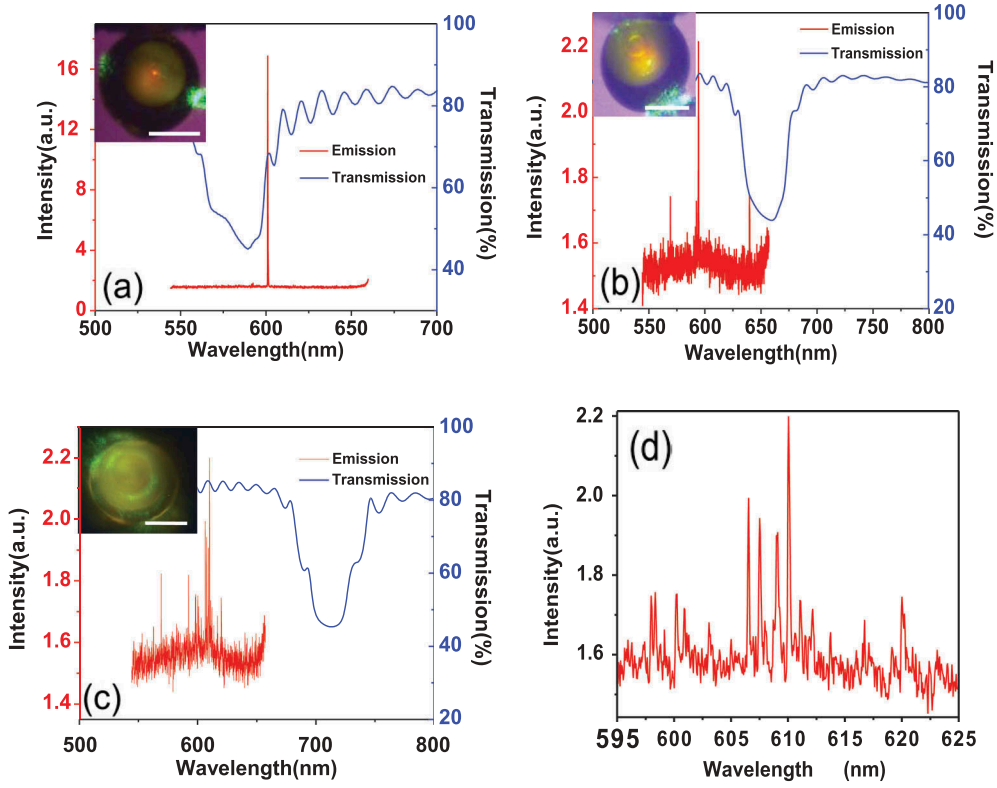

Figure 4. (Colour online) Lasing (red lines) and transmission (blue line) spectra of the pumped LDDCLC microspheres with different chiral dopant concentrations. (a) 24wt%, (b) 22wt% and (c) 20wt%. The top left insets show microscopy images of the pumped LDDCLC microspheres and (d) The expanded spectrum of LDDCLC microsphere with 20wt% R811 in the range of 595–625 nm. The scale bar is 50 μm.

the reflection band is excited, as shown in Figure 4(a). If the LDDCLC microsphere with 22wt% R811 is adopted, the pitch length will become longer, and the long-wavelength edge of the reflection band will move out of the fluorescence emission wavelength range of DCM, whereas the short-wavelength edge of the reflection band will shift into it. As shown in Figure 4(b), BWGM emerges, and PBG at the short-wavelength edge of the reflection band appears with a very low intensity because the wavelength of PBG is a little far from the emission wavelength range. To obtain a higher Bragg mode, the pitch is further increased by reducing the concentration of the chiral dopant (20wt% R811). However, the Bragg mode is barely visible (Figure 4(c)). This result can be explained by the Bragg reflection theory. The reflectivity of the CLC layer (R) can be approximately got by [28]:

$$R \approx \left(\frac{1 - e^{-2\Delta n\pi h/\overline{n}p}}{1 + e^{-2\Delta n\pi h/\overline{n}p}}\right)^2 \quad (1)$$

where $\overline{n}$ is the average refractive index of LCs and h is the thickness of the layer. Eq. 1 shows that R reduces with the increase of the pitch length and the decrease of Δn. Since this LDDCLC has a long helical pitch and a very low Δn (0.083), the periodic Bragg structure has not enough ability to limit the fluorescence within the CLC microdroplet. As a result, the formation mechanism of this WGM was consistent with WGM2 in Figure 3(b). Under high intensity pump lasing, the fluorescence was generated and formed the WGM at the air and PG2 interface. Therefore, only a weak WGM is observed in Figure 4(c).

We use HDDCLC (26 wt% R811) microsphere to measure the excitation threshold of the Bragg mode and WGM. Both Bragg and WGM lasing emissions are enhanced with the increase of the pumping pulse energy, as shown in Figure 5. When the pumping pulse energy is above the thresholds, i.e. 1.8 μJ for Bragg modes and 2.2 μJ for WGMs, the emission intensities rapidly increase, which confirms the realisation of Bragg lasing modes and WGMs [29]. However, the Bragg modes are more efficient than WGMs.

4. Conclusion

In conclusion, this study demonstrates, for the first time, the optical-pumped lasing emission of a DDCLC microdroplet-PG2-HGM microsphere. Different lasing modes including PBG, BWGM and WGM are obtained by changing the concentration of the chiral dopant and the refractive index of LC. For

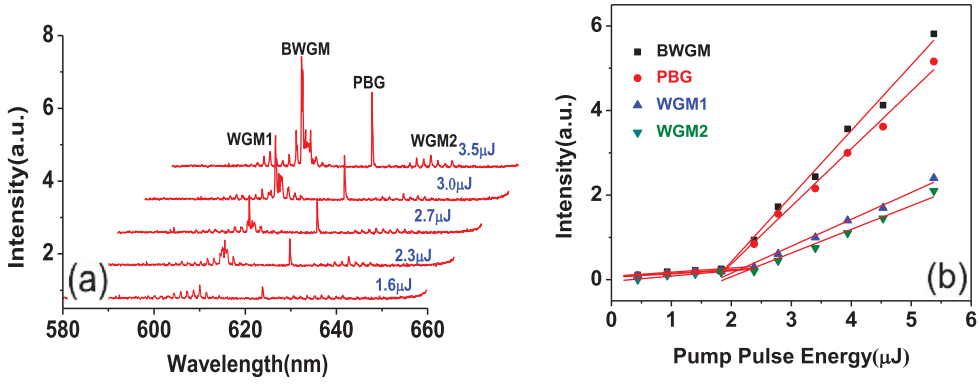

Figure 5. (Colour online) (a) Lasing spectra of a CLC microsphere pumped by different pulse energies. (b) Lasing intensity as a function of the input pumping pulse energy.

HDDCLC microspheres, three types of emissions are observed: PBG and WGM (28wt% R811); PBG, WGM and BWGM (26wt% R811); WGM and BWGM (23wt% and 20wt% R811). Moreover, the experimental results show that the bright ring diameter of BWGM enhances with the increase of the pitch length. For LDDCLC microspheres, a single PBG can be achieved when the reflection band is around 600 nm (24wt% R811), BWGM appears when the chiral dopant concentration is 22wt%, and when the chiral dopant concentration drops to 20wt%, the low reflectivity of the CLC layer causes BWGM to disappear. These findings provide a new idea for designing DDCLC microlasers with various output modes and have potential applications in sensors and tunable optical devices.

Disclosure statement

No potential conflict of interest was reported by the authors.

Funding

This work was financially supported by the National Science Foundation of China (Grant No.U1531102, 11603008, 61107059), and the Fundamental Research Funds for the Central Universities (HEUCF181116).

References

[1] Uchida T. 40 years reseach and development on liquid crystal displays. Jpn J Appl Phys. 2014;53:03CA02.
[2] Wang FR, Liu YJ, Lu YL, et al. High-sensitivity Fabry Perot interferometer temperature sensor probe based on liquid crystal and the Vernier effect. Opt Lett. 2018;43(21):5355–5358.
[3] Wang FR, Wang JL, Long SB, et al. All-fibre one-way filter based on both-end-filled photonic liquid crystal fibres. Liq Cryst. 2017;45(7):1004–1009.
[4] Lu YL, Yang Y, Wang Y, et al. Tunable liquid-crystal microshell-laser based on whispering-gallery modes and photonic band-gap mode lasing. Opt Express. 2018;26(3):3277–3285.
[5] Lin JD, Hsieh MH, Wei GJ, et al. Optically tunable/switchable omnidirectionally spherical microlaser based on a dye-doped cholesteric liquid crystal micro-droplet with an azo-chiral dopant. Opt Express. 2013;21(13):15765–15776.
[6] Huang Y, Zhou Y, Doyle C, et al. Tuning the photonic band gap in cholesteric liquid crystals by temperature-dependent dopant solubility. Opt Express. 2016;14(3):1236–1242.
[7] Lin SH, Lee CR. Novel dye-doped cholesteric liquid crystal cone lasers with various birefringences and associated tunabilities of lasing feature and performance. Opt Express. 2011;19(19):18199–18206.
[8] Chanishvili A, Chilaya G, Petriashvili G, et al. Widely tunable ultraviolet-visible liquid crystal laser. Appl Phys Lett. 2005;86(5):051107.
[9] Tzeng SYT, Chen CN, Tzeng Y. Thermal tuning band gap in cholesteric liquid crystals. Liq Cryst. 2010;37(9):1221–1224.
[10] Furumi S, Yokoyama S, Otomo A, et al. Electrical control of the structure and lasing in chiral photonic band-gap liquid crystals. Appl Phys Lett. 2003;82(1):16–18.
[11] Lin TH, Jau HC, Chen CH, et al. Electrically controllable laser based on cholesteric liquid crystal with negative dielectric anisotropy. Appl Phys Lett. 2006;88(6):061122.
[12] Seok LS, Bin KJ, Ho KY, et al. Wavelength-tunable and shape-reconfigurable photonic capsule resonators containing cholesteric liquid crystals. Sci Adv. 2018;4:eaat8276.
[13] Shibaev PV, Sanford RL, Chiappetta D, et al. Light controllable tuning and switching of lasing in chiral liquid crystals. Opt Express. 2005;13(7):2358–2363.
[14] Chilaya G, Chanishvili A, Petriashvili G, et al. Reversible tuning of lasing in cholesteric liquid crystals controlled by light-emitting diodes. Adv Mater. 2007;19(4):565–568.
[15] Jung YD, Khan M, Park SY. Fabrication of temperature- and pH-sensitive liquid-crystal droplets

with PNIPAM-b-LCP and SDS coatings by microfluidics. J Mater Chem B. 2014;2:4922–4928.
[16] Humar M, Ravnik M, Pajk S, et al. Electrically tunable liquid crystal optical microresonators. Nat Photonics. 2009;3(10):595–600.
[17] Wang Y, Zhao LY, Wang L, et al. Detecting enzymatic reactions in penicillinase via liquid crystal microdroplet-based pH sensor. Sens Actuators B. 2018;258:1090–1098.
[18] Xu Y, Liang W, Yariv A, et al. Modal analysis of Bragg onion resonators. Opt Lett. 2004;29(5):424–426.
[19] Humar M, Muševič I. 3D microlasers from self-assembled cholesteric liquid-crystal microdroplets. Opt Express. 2010;18(26):26995–27003.
[20] Pirnat G, Humar M, Muševič I. Remote and autonomous temperature measurement based on 3D liquid crystal microlasers. Opt Express. 2018;26 (18):22615–22625.
[21] Wang Y, Li HY, Zhao LY, et al. Tunable whispering gallery modes lasing in dye-doped cholesteric liquid crystal microdroplets. Appl Phys Lett. 2016;109 (23):231906.
[22] Lin HB, Eversole JD, Campillo AJ. Spectral properties of lasing microdroplets. J Opt Soc Am B. 1992;9 (1):43–50.
[23] Mazumder MM, Gillespie JB, Chen G, et al. Wavelength shifts of dye lasing in microdroplets: effect of absorption change. Opt Lett. 1995;20(8):878–880.
[24] Xu F, Crooker PP. Chiral nematic droplets with parallel surface anchoring. Phys Rev E. 1997;56 (6):6853–6860.
[25] Cipparrone G, Mazzulla A, Pane A, et al. Chiral self-assembled solid microspheres: a novel multifunctional microphotonic device. Adv Mater. 2015;23(48):5704.
[26] Zhou Y, Huang Y, Wu ST. Enhancing cholesteric liquid crystal laser performance using a cholesteric reflector. Opt Express. 2006;14(9):3906–3916.
[27] Humar M. Liquid-crystal-droplet optical microcavities. Liq Cryst. 2016;43:1937–1950.
[28] Yang DK, Wu ST. Fundamentals of liquid crystals devices. Chichester: John Wiley & Sons Ltd; 2006.
[29] Ta VD, Chen R, Sun HD. Tuning whispering gallery mode lasing from self-assembled polymer droplets. Sci Rep. 2013;3(1):1362